Available online at www.sciencedirect.com
SCIENCE DIRECT®
Journal of the European Ceramic Society 26 (2006) 259–266
www.elsevier.com/locate/jeurceramsoc

Elaboration and mechanical characterization of nanocomposites thin films Part I: Determination of the mechanical properties of thin films prepared by in situ polymerisation of tetraethoxysilane in poly(methyl methacrylate)

Fayna Mammeri[a,b], Eric Le Bourhis[b], Laurence Rozes[a], Clément Sanchez[a,*]

[a] *Université Pierre et Marie Curie, Laboratoire de Chimie de la Matière Condensée, UMR 7574 CNRS, Case 174, 4 Place Jussieu, 75252 Paris Cedex 05, France*
[b] *Université de Poitiers, Laboratoire de Métallurgie Physique, UMR 6630 CNRS, SP2MI-Téléport 2-Bd Marie et Pierre Curie, B.P. 30179, 86962 Futuroscope-Chasseneuil Cedex, France*

Received 25 July 2004; received in revised form 10 November 2004; accepted 21 November 2004
Available online 21 January 2005

Abstract

The sol–gel process allows to design hybrid organic–inorganic materials constituted by organic molecules or macromolecules and inorganic metal oxo-polymers interpenetrated at the nanometer scale. These hybrids were deposited as functional coatings with tunable thickness on float glass substrates. Good adhesion and mechanical behaviour of the coatings are required to keep their functionality in time hence; the performance of the PMMA-SiO_2 based thin films was investigated using nanoindentation. This study validates nanoindentation measurements as an appropriate technique to characterize hybrid organic–inorganic thin films, despite visco-elastic behaviours. Specific analysis procedures and the use of appropriate models allowed us to determine the indentation modulus and hardness of the hybrid layers reproductively. The structure and the mechanical behaviour are reported for thin films as a function of the fraction of silica.

Keywords: Nanocomposites; Mechanical properties; Sol–gel processes; Films; Nanoindentation; SiO_2; TEOS

1. Introduction

Surface coatings represent a flexible and economic mean to protect or modify the functional behaviour of a glass component without having to modify its composition. Good adhesion and mechanical behaviour are also required to keep the functionality in time. Several techniques, like sputtering or chemical-vapor deposition, allow to process coatings but are mostly dedicated to flat substrates like glazings. In contrast, the sol–gel process is very attractive and versatile to prepare inorganic or hybrid films with tunable thickness.[1]

The sol–gel process involves a chemistry based on inorganic polymerisation; precursors are usually metallo-organic compounds such as alkoxides: $M(OR)_n$ (M = Si, Ti, Zr, Al, ... and $OR = OC_nH_{2n+1}$). Hydrolysis and condensation reactions lead to the formation of a metal-oxo based macromolecular network.[1] Moreover, mild synthetic conditions provided by sol–gel chemistry allow to incorporate organic components into the inorganic network, producing hybrid organic–inorganic materials that allow to combine the properties of both polymer and oxide materials.[2–5] For example, the mechanical properties can be tuned between those of glasses and those of polymers by tuning the initial composition of the different precursors.[6–11]

Instrumented nanoindentation has become widely used to test thin solid films. Recently, this technique was applied

* Corresponding author. Tel.: +33 1 44 27 55 34; fax: +33 1 44 27 47 69.
E-mail address: clems@ccr.jussieu.fr (C. Sanchez).

0955-2219/$ – see front matter © 2004 Elsevier Ltd. All rights reserved.
doi:10.1016/j.jeurceramsoc.2004.11.013

to measure the mechanical properties of sol–gel derived hybrid thin films based on silica nanoparticles mixed with methyltrimethoxysilane,[12] silica-epoxy,[9,11,13] or nanoparticles dispersed in a poly(methacrylate) based matrix.[14] The nanoindentation technique allows to investigate the elastic, plastic and viscous responses of hybrid coatings. Dedicated procedures may allow to investigate as well their brittle behaviour and adhesion to the glass substrate.[15,16] In order to answer practical applications, scratch-test and Taber test are being used to evaluate the durability of the coatings.[17,18]

In the present paper, we have investigated the mechanical response of PMMA-silica hybrid thin films with increasing molar fraction of silica, which was generated by in situ polymerisation of TEOS in PMMA. In order to determine reproducibly the indentation modulus and hardness, specific indentation procedures are to be used and presented. Indeed, a careful analysis of the loading–unloading curves is required as soon as the duration of the test and the characteristic relaxation time of the material are of the same order.

2. Experimental procedures

2.1. Elaboration of the films

2.1.1. Chemicals

Tetraethoxysilane (TEOS 99%) and [3-(methacryloxy) propyl]triethoxysilane (MPTES) were purchased from ABCR-Gelest, azobisisobutyronitrile (AIBN) from Fluka. The monomer methyl methacrylate (MMA 99% from Aldrich) was purified by distillation before use. Acetonitrile was dried over molecular sieve.

2.1.2. Preparation of the PMMA-SiO_2 hybrid thin films

Trialkoxysilyl-functionalized poly(methyl methacrylate) was synthesized by copolymerisation of 0.4 mol of methyl methacrylate, [CH_2=CCH_3COOCH_3] and 2.08×10^{-2} mol of methacryloxypropyltriethoxysilane, [CH_2=$CCH_3COO(CH_2)_3Si(OEt)_3$] via a free radical process using a thermal initiator (1 wt.% AIBN, in acetonitrile, 70 °C for 24 h in argon atmosphere). The resulting functionalized PMMA was purified by precipitation in methanol.

Hybrid solutions were obtained by adding various quantities (Table 1) of pre-hydrolyzed tetraethoxysilane, TEOS, (H_2O/Si = 4, in acidic conditions, with 1 mol l^{-1} HCl, pH 1) to a solution of functionalized PMMA in THF (concentration of 1 g l^{-1}).

The sols were vigorously stirred at room temperature for 48 h before deposition by spin-coating on standard float glass (Saint-Gobain). Before deposition, the substrates were cleaned using a soap solution, followed by rinsing in demineralized water allowing to obtain an hydrophilic surface. After deposition, the samples were cured at 100 °C for 8 h to complete the silica condensation.

2.2. Structural characterizations

FTIR spectra (Magna IR 550 Nicolet, 32 scans, 4 cm^{-1} resolution) were taken before and after the polymerisation of the triethoxysilane functionalized PMMA. Dry powders were spread into KBr pellets.

The molecular weight of the polymer was determined by Size Exclusion Chromatography (SEC) in THF at a flow rate of 0.8 ml/min and using a PMMA standard calibration curve (Waters apparatus); the porosity of the μ-styragel columns was 10^5, 10^4, 10^3, 500 and 100 Å.

Modulated Differential Scanning Calorimetry (DSC) was performed with a TA Instruments DSC 2920 thermal analyzer; the heating rate was 5 °C/min to measure the glass transition temperature (T_g) and the variation of calorific capacity (ΔC_p) of the PMMA in the hybrid nanocomposites. Thermogravimetric analysis (TGA) performed on the xerogels revealed the organic to inorganic ratio; the heating rate was 10 °C/min. All the thermal analysis were performed in oxygen and nitrogen atmospheres.

NMR experiments in solution were carried out on a AV400 Brucker spectrometer; 10 mm tubes were used with an inner 8 mm tube containing tetramethylsilane (TMS) as a reference and $CDCl_3$ as deuterated solvent. ^{29}Si sites will be labelled with the conventional T_n and Q_n notations. T_n refers to trifunctional $Si(OEt)_3$ units and Q_n to tetrafunctional $Si(OEt)_4$ units, n is the number of bridging O atoms surrounding one Si. ^{29}Si CP MAS solid-state NMR data were recorded on a AV300 Brucker spectrometer (59.62 MHz) using 7 mm diameter zircona rotors at a spinning frequency of 4 kHz.

Chemical analysis were performed by the Laboratoire Central of the National French Research Council (CNRS) in Vernaison, France.

The hybrid layer thickness was determined on cross-sectional images obtained in a Leo Gemini DSM 982 Scanning Electron Microscope (with Gun Field) and is the average of four different measurements.

Table 1
Samples chemical characteristics (PMMAX where X is the functionalized PMMA, noted f-PMMA, molar ratio)

Sample	Composition (wt.% f-PMMA)	Glass temperature T_g (°C)	Heat capacity variation ΔC_p (J g^{-1} °C^{-1})
PMMA100	100	105	0.290
PMMA75	78	111	0.220
PMMA50	53	156	0.037
PMMA25	28	–	–

2.3. Mechanical characterization

The residual stresses in the coatings were determined from the change in spherical curvature of a thin circular glass substrate using a Dektak surface profiler before and after deposition of the coatings. The curvature was measured along two orthogonal directions over the central area. Then, the average stress was calculated from a modified version of Stoney's equation[19,20] using elastic modulus $E = 73 \pm 1$ GPa and Poisson's ratio $\nu = 0.23$ for the glass substrate.[21]

The samples were deformed by a Berkovich diamond pyramid using a NanoHardness Tester machine from CSEM (Switzerland). The calibration procedure suggested by Oliver and Pharr[22] was used to correct for the load-frame compliance of the apparatus and the imperfect shape of the indenter tip. The area function $A(h_c)$ was calibrated on fused silica and relates the contact area to the contact depth h_c. The tests were performed at room temperature in the force-control mode of the machine. Maximum loads were ranged between 0.25 and 50 mN to extract the hardness and indentation modulus of the films; five indentations were made for each load. We used two loading procedures. Firstly a load–reload sequence and secondly a load–hold–rapid unloading sequence were used to control creep (induced by the presence of PMMA) during unloading; otherwise, the conventional Oliver and Pharr procedure could not be used to determine the mechanical properties.[15,16] The load–displacement curves were analysed using the method proposed by Oliver and Pharr,[22] yielding the reduced indentation modulus (E_r) and the hardness ($H = F/A(h_c)$) by fitting the last unloading curve.

Taber abrasion experiments were done in order to quantify the resistance to fracture and adhesion behaviour of the hybrid layers and to correlate with fracture patterns under large indentation loads (300 mN). Abrasion index is defined by the measure of the turbidity, which increased when delamination of the film is induced under the mechanical solicitation.

3. Results and discussion

3.1. Description of the layers

The polymerisation reaction of the vinylic groups was performed by a free radical polymerisation; the reaction can be represented by Scheme 1.

All the features induced by the formation of polymer chains can be followed by infrared (IR) spectroscopy: the disappearance of the methacrylate $\nu_{C=C}$ band at 1638 cm^{-1} is related to the saturation of the vinylic bond $^1C{=}^3C$ whereas the shift of the carbonyl $\nu_{C=O}$ band from 1725 to 1735 cm^{-1} is a consequence of the loss of conjugation with the C=C bond during the conversion of the monomer in polymer. ^{13}C CP MAS NMR was used to check the conversion of all methyl methacrylate in PMMA (Fig. 1); indeed, IR spectroscopy only allows to observe the decrease of the C=C band. When polymerisation occurs, the peaks due to the vinylic groups (C_3 and C_1 at 136 and 125 ppm, respectively) disappear whereas two new peaks appear, at 45 ppm due to the quaternary carbon (C_{3p}) and at 177 ppm due to the non-conjugated C=O groups (C_{4p}).

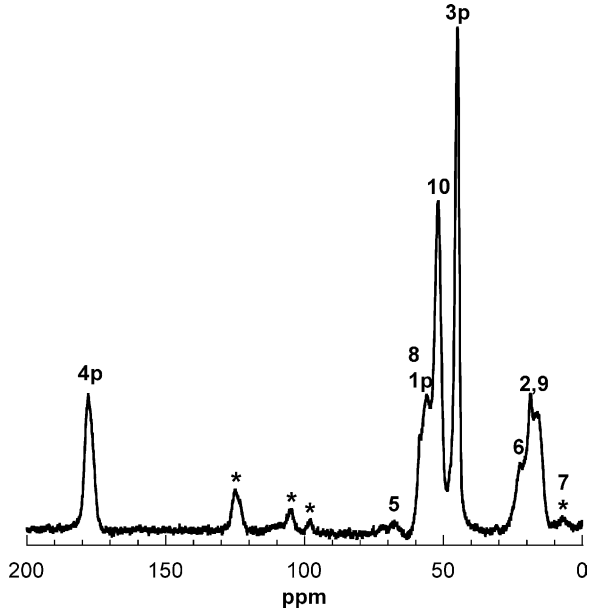

Fig. 1. ^{13}C CP MAS NMR spectra of triethoxysilane functionalized PMMA. (*) spinning size bands.

The ^{29}Si NMR experiments recorded in solution of the functionalized PMMA exhibit a single peak at −47 ppm assigned to T_0 units, allowing us to confirm the conservation of $Si(OEt)_3$ groups of the coupling agent during the polymerisation reaction: they are neither condensed nor hydrolyzed. Consequently, the triethoxysilane functional groups are hydrolytically stable and the polymer does not cross-link upon exposure to moisture. Moreover, the experimental silicon to carbon weight ratio, obtained from chemical analysis, is in good agreement with the theoretical one ($Si/C_{exp} = 0.021$ and $Si/C_{th} = 0.025$). Therefore, the functionalized PMMA

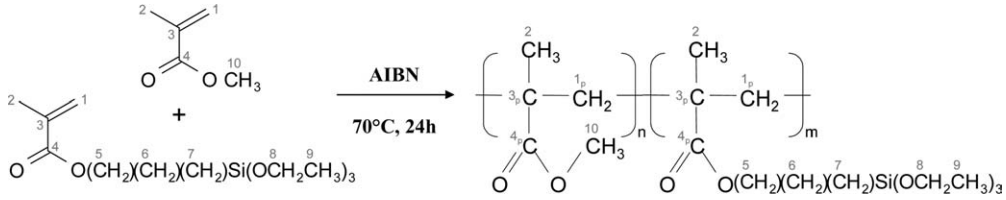

Scheme 1.

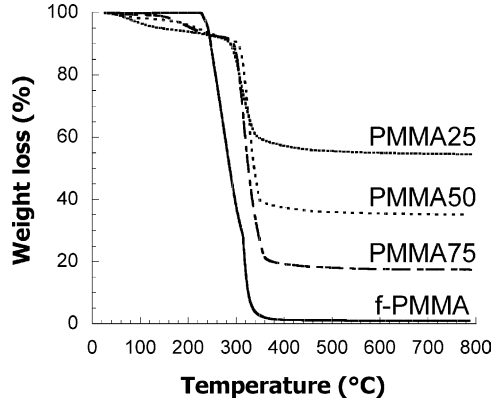

Fig. 2. TGA curves under O_2 atmosphere of functionalized PMMA and hybrid materials: (a) f-PMMA, (b) PMMA75, (c) PMMA50 and (d) PMMA25.

(f-PMMA) is a PMMA-MPTES copolymer with about 5% of triethoxysilane groups. Molecular weight of the functionalized PMMA was determined to be $M_w = 55{,}000\ g\ mol^{-1}$ and polydispersity index was lower than 2.

Optical transparency is a first criterion for the formation of a homogeneous phase of both inorganic and organic constituents. In fact, no opacity of the coating, which could be attributed to a macroscopic phase separation and to the formation of large domains of inorganic component, was observed. Moreover, the observation of the films cross-sections in the backscattered electrons mode of the SEM never showed any microscopic phase separation, in good correlation with the optical aspect of the films. Consequently, we could conclude that all the prepared thin films were homogeneous at the micronic scale as all of them were transparent. Moreover, SEM experiments allowed us to measure the layers thicknesses; all were ranged between 1.5 and 2 μm.

Thermogravimetric analysis (TGA) performed under O_2 atmosphere on the xerogels revealed that the organic to inorganic ratios were in good agreement with the sol compositions, assuming the full condensation of $Si(OEt)_4$ in pure silica SiO_2. Loss weight curves were very similar under both O_2 and N_2 atmospheres. Consequently, it is concluded that all the PMMA is decomposed under inert atmosphere. The onsets of the thermal decomposition of all hybrid materials were about 50 °C higher than for the neat functionalized PMMA but no improvement of the thermal stability was observed when the silica content was increased (Fig. 2). The combination of two events may explain why the thermal stability is independent on the organic to inorganic ratio: the silica component induced a protective barrier against thermal degradation for organic species[23] (hydrogen bondings SiOH···O=C were established between silica and PMMA) but promoted simultaneously the propagation of thermal energy[24] (indeed, its thermal conductivity is about 10 times larger than that of PMMA).

Modulated differential scanning calorimetry (DSC) performed on the functionalized PMMA allowed to measure the glass transition temperature as well as the heat capacity variation: $T_g = 105\ °C$ and $\Delta C_p = 0.290\ J\ g^{-1}\ °C^{-1}$. An increase in T_g was observed when the silica content was increased in the hybrid materials: $T_g = 111$ and 156 °C for PMMA75 and PMMA50, respectively (Table 1). For the silicon-rich coatings (PMMA25), the DSC curve did not show any relevant thermal effects up to 250 °C.

This increase in T_g (from 105 to 156 °C) simultaneously to the decrease in ΔC_p (from 0.290 to 0.037) when the silica content is increased (from 0 to 25 mol%) may be explained by a decrease of the polymer mobility due to the progressive confinement of the polymer by the silica network, and because of the increase of cross-linking between organic and inorganic components. For high silica loading the PMMA chains must be highly confined by the silica network and this decrease in mobility yields to a strong blurring of the T_g transition.[25]

3.2. Time dependence of the indentation behaviour of hybrid coatings

The mechanical response of hybrid PMMA-SiO_2 thin films showed a time dependence due to the presence of PMMA.[26] Even though, the non-elastic part during the unloading of the indenter can be limited by a suitable procedure: a load–reload sequence[16] or a load–hold–rapid unloading sequence (Fig. 3). The unloading curve has to be carefully analysed as it is not purely elastic despites no nose was observed.[16,27,28] In fact, when the unloading curve is fitted by a power law following Oliver and Pharr:[22]

$$F = A(h - h_r)^m \quad (1)$$

where F is the applied load, A is a constant and h_r is the residual depth, the power factor m is found to be beyond 2 while it is expected to range between 1.2 and 1.6 for purely

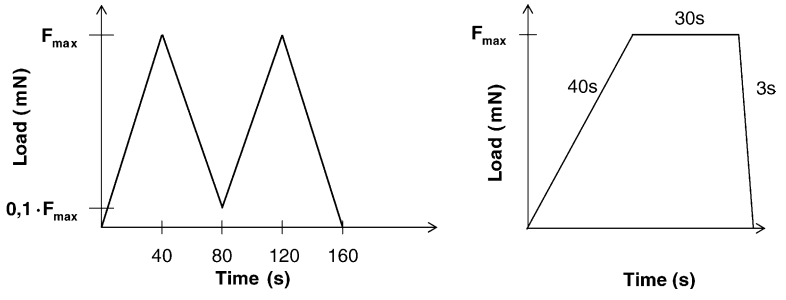

Fig. 3. Indentation procedures: (a) load–reload sequence and (b) load–hold–rapid unloading sequence.

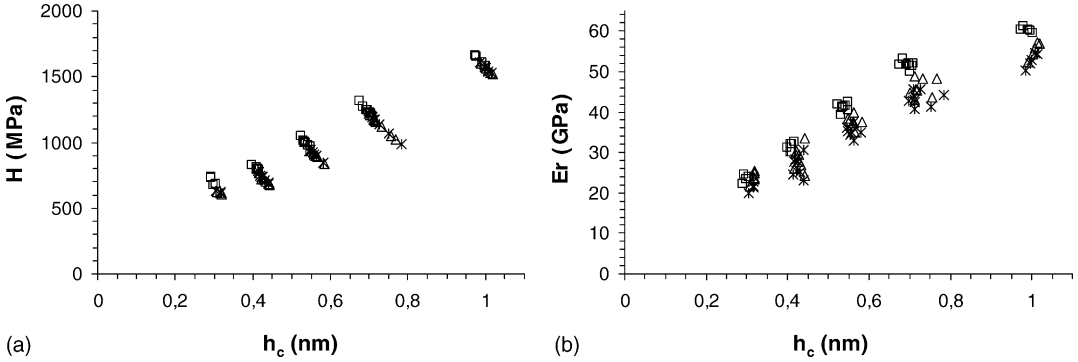

Fig. 4. (a) Hardness (H), (b) indentation modulus (E_r) as a function of the indentation depth (h_c) for PMMA75 hybrid: (□) load–reload sequence, (Δ) load–hold–rapid unloading sequence, (*) load–hold–rapid unloading corrected by the procedure proposed by Tang and Ngan.[27]

elastic unloading. Consequently, even though a nose is not observed in the unloading curve, a 3 s unloading period is long enough to detect non-elastic effects. Hence, the mechanical properties have to be corrected as suggested by Tang and Ngan.[27]

When a hold–rapid unloading sequence is used, the creep rate of the material can be estimated during the hold period and used to correct the contact stiffness $S = \mathrm{d}F/\mathrm{d}h$ following Tang and Ngan:[27]

$$\frac{1}{S_c} = \frac{1}{S} + \frac{\dot{h}_h}{\dot{F}_u} \tag{2}$$

where S_c is the corrected stiffness, while S is the experimental one. $\dot{h}_h = \mathrm{d}h_h/\mathrm{d}t$ is the penetration rate of the indenter during the hold period and $\dot{F}_u = \mathrm{d}F_u/\mathrm{d}t$ is the unloading rate. Under our experimental conditions, S_c was found to be affected by about 5% while the indentation depth h_c was only slightly modified by this correction. It is concluded that under our experimental conditions, both the indentation modulus and the hardness are affected by viscoelastic effects to a magnitude lower than 10% (see Fig. 4).

Time-dependence of the mechanical response is observed when the loading and unloading times are not negligible as compared to the relaxation time. Viscous flow is induced by the presence of the polymer component. To predict the mechanical behaviour of hybrid materials, the viscous penetration of the indenter has to be considered and added to the elastic and plastic deformations. An interesting prediction of the viscous elastic plastic (VEP) model is that the responses are controlled by total rise time and not by the loading rate.[28] Hence, we decided to use a total time of test constant.

The VEP model and its application to hybrid materials were described and reported earlier.[29] Particularly, we showed that the relaxation time was a pertinent parameter to predict the time dependence (Fig. 5). An increase in relaxation time with increasing silica content was determined for the hybrid materials in the whole range of compositions investigated here and is due to an attenuation of the polymer mobility. This attenuation was already highlighted by DSC measurements as a decrease in ΔC_p and an increase in T_g was determined when the silica content was increased.

3.3. Layers mechanical properties

All the measured average residual stresses were below 25 MPa; therefore, the coatings were only slightly constrained in tension. All thin films were tested using the load–reload sequence. Fig. 6 depicts the evolution of the indentation modulus and the hardness as a function of the contact indentation depth h_c (scaled with the coating thickness) for the studied PMMA-SiO_2 hybrid materials.

The increase in the mechanical properties as the indentation depth increases results from the strong influence of the substrate. This means that the mechanical responses are dominated by thin films properties at low indentation depths whereas those determined at larger indentation depths are substrate dependent. Various models have been suggested to describe the combinated influence of both the substrate and the coating allowing to calculate the sole mechanical response of the thin film.

Mencik et al.[30] compared five models to predict the indentation modulus of homogeneous thin films on a substrate. One of them (the reciprocal exponential function) was found to be the most suitable; it follows Doerner and Nix suggestion to consider the film and substrate as two springs in series[31] and is given by:

$$\frac{1}{E_r} = \frac{1}{E_s} + \left(\frac{1}{E_f} - \frac{1}{E_s}\right) \exp\left(-\beta \frac{h_c}{e}\right) \tag{3}$$

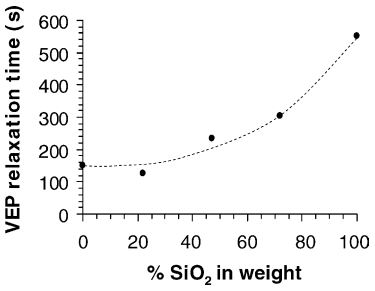

Fig. 5. VEP relaxation time as a function of the silica content for PMMA-silica (obtained from in situ polymerization of TEOS in PMMA).

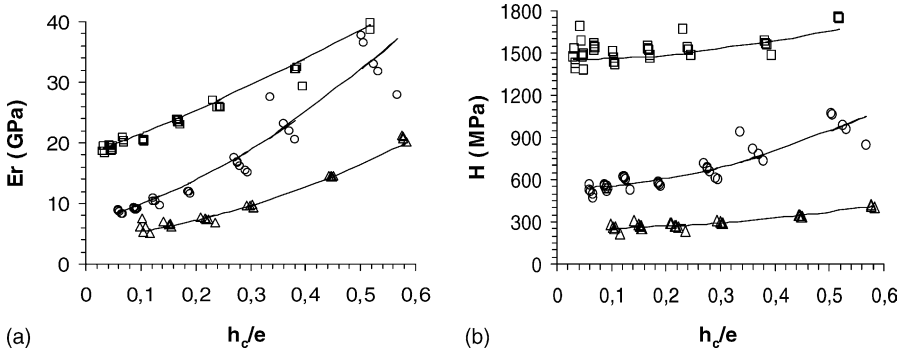

Fig. 6. (a) Indentation modulus (E_r) and (b) hardness (H) as a function as indentation depth, scaled with the coating thickness h_c/e for samples (□) pure sol–gel silica, (○) PMMA50 and (△) PMMA100. The model curves are continuous lines.

where s and f subscripts are for the substrate or the film respectively. E_r denotes the measured substrate-film composite property. The substrate indentation modulus was determined separately by carrying out experiments on an uncoated substrate: $E_s = 80 \pm 4$ GPa in relatively good agreement with expected value from the literature ($E_s = E/(1-\nu^2) = 77 \pm 1$ GPa).[21,32] Then, the unknowns (E_f, β) were determined by subtracting $1/E_s$ to $1/E_r$ and applying the least-square method to the logarithms as suggested by Mencik et al.[30]

A similar procedure was applied to determine the hardness of the films. In fact, the combined contributions of the coating and the substrate are measured. However, at equal indentation depth, the influence of the substrate on the measured hardness is lower than on the indentation modulus. Indeed, the plastic strain field is much less extended spatially than the elastic strain field. We retained the exponential law proposed by Bhattacharya and Nix:[33]

$$H = H_s + (H_f - H_s)\exp\left[-\alpha\left(\frac{h_c}{e}\right)^n\right] \quad (4)$$

For soft coatings on hard substrates, $n = 2$. H_s was determined on the uncoated glass: $H_s = 8.1 \pm 0.4$ MPa in good agreement with Dériano et al.;[32] thus H_f and α could be determined using a least-square method to the logarithms similarly as above for the indentation modulus.

These equations do not take into account the influence of fracture. These models could be applied to the studied thin films, because PMMA-SiO_2 hybrid materials may present this kind of mechanical behaviour only above large critical loads, beyond the range used here to extract the film properties.[26] Calculated values of indentation modulus and hardness for the different samples are gathered in Table 2. They allowed us to determine the mechanical response of the sole thin film without substrate influence as a function of composition. The trends are found in good agreement with layers composition since an improvement of both the indentation modulus and the hardness versus the silica content is observed. For instance, PMMA25 hybrid samples containing about 30% of PMMA showed indentation modulus (9.5 ± 1.00 GPa) and hardness (0.85 ± 0.09 GPa) improved by a factor 2.3 and 3.4 respectively with respect to the values measured for the PMMA reference sample.

The mechanical properties of a composite material (here the organic–inorganic hybrid) can be modeled by:[9]

$$E_{linear} = \tau_{PMMA} E_{PMMA} + \tau_{Silica} E_{Silica} \quad (5)$$

$$\frac{1}{E_{reciprocal}} = \frac{\tau_{PMMA}}{E_{PMMA}} + \frac{\tau_{Silica}}{E_{Silica}} \quad (6)$$

$$H_{composite} = \tau_{PMMA} H_{PMMA} + \tau_{Silica} H_{Silica} \quad (7)$$

where τ is the volumic fraction of PMMA or silica. Assuming that the densities of PMMA and silica were the following: $\rho_{PMMA} = 1.2\ g\,cm^{-3}$ and $\rho_{Silica} = 2\ g\,cm^{-3}$, we could calculate the indentation modulus and hardness for the PMMA-SiO_2 hybrid materials (Fig. 7). Mechanical properties of the hybrid materials were found to be well predicted with a linear model Eqs. (5)–(7) while Etienne et al.[9] report intermediate situation for the elastic properties. This result shows that a nano-sized composite allows for reaching strong improvement of the mechanical behaviour and this might be attributed to the large hybrid interfaces, which could be developed in the hybrid nanocomposite materials as the inorganic component is generated in situ in a preformed polymer. The influence of the size of the hybrid interface on the mechanical properties is discussed in more details in the part II paper.

3.4. Adhesion and fracture of the coatings under high loads

During an indentation test, various kinds of mechanical failure (as cracking or delamination) may occur in the coating or at the interface between substrate and coating. All

Table 2
Sample mechanical characteristics

Sample	Thickness (nm)	E (GPa)	H (GPa)
f-PMMA	1790	4.10 ± 0.40	0.25 ± 0.03
PMMA75	1680	7.60 ± 0.80	0.50 ± 0.05
PMMA50	2030	6.60 ± 0.70	0.54 ± 0.06
PMMA25	1890	9.50 ± 1.00	0.85 ± 0.09
Sol–gel silica	2190	17.50 ± 2.00	1.5 ± 0.15

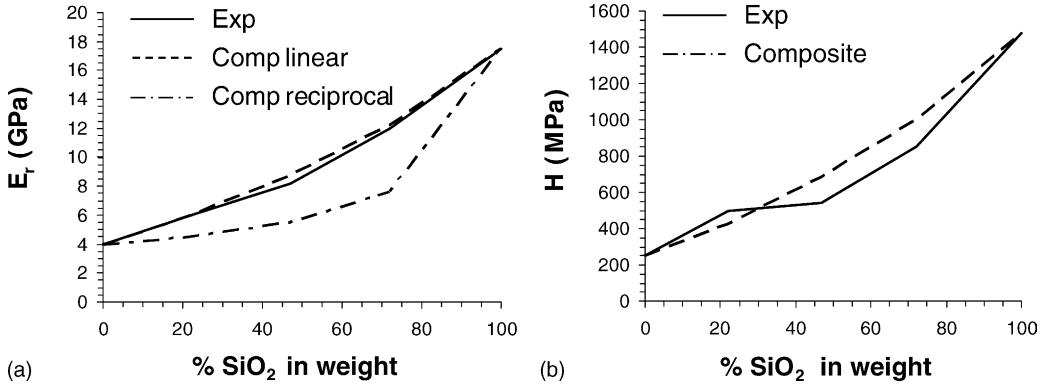

Fig. 7. Mechanical properties of the films (continuous lines are experimental data) were obtained from the best fit of the experimental data (Eqs. (3) and (4)). Dashed lines are calculated using Eqs. (5)–(7).

these features result in typical changes in the loading curve. For inorganic sol–gel coatings, Malzbender[12] analyzed the fracture evolution as a function of the applied indentation load. At low loads, radial cracking may occur. As the load increases, delamination of the coating from the substrate may occur leading to chipping (or removal of pieces of coating) under even larger loads.

Using optical microscopy after applying a load of 300 mN on the hybrid thin films, we observed various phenomena depending on the silica to polymer ratio (Fig. 8). For a silica-rich coating (PMMA25), delamination at the interface occurred, leading to the layer chipping, because of the propagation of cracks at the interface between the substrate and the layer and towards the surface of the coatings. This behaviour was detected on the loading curve as an abrupt change in slope. For coatings with increasing organic phase (PMMA50 and PMMA75), delamination was observed but no chipping occurred. Delamination was revealed by irisations around the indent site and by a slight change in the slope of the loading curve (Fig. 8). Finally, for the sample with the highest PMMA ratio (f-PMMA), neither delamination nor chipping occurred.

Interestingly, the same trends were observed when a lateral movement was added to the tip (nanoscratch test under a load of 350 mN). Only a plastic deformation was observed in the PMMA75 coating, while delamination was observed for the PMMA25 coating. Taber performances of the hybrid layers were found to be also in good correlation with the indentation observations. In fact, the abrasion resistance was improved when the silica content was increased (Fig. 9). A PMMA25 thin film (500 nm) could resist near 80 revolutions whereas PMMA75 film delamination occurred after 25 revolutions. Noticeably, the performance to Taber test is drastically improved when the thickness of the coating is increased. In fact, the abrasion resistance of the PMMA25 coating is raised from 80 revolutions to near 550 revolutions when the thickness of the film is increased by a factor 4.

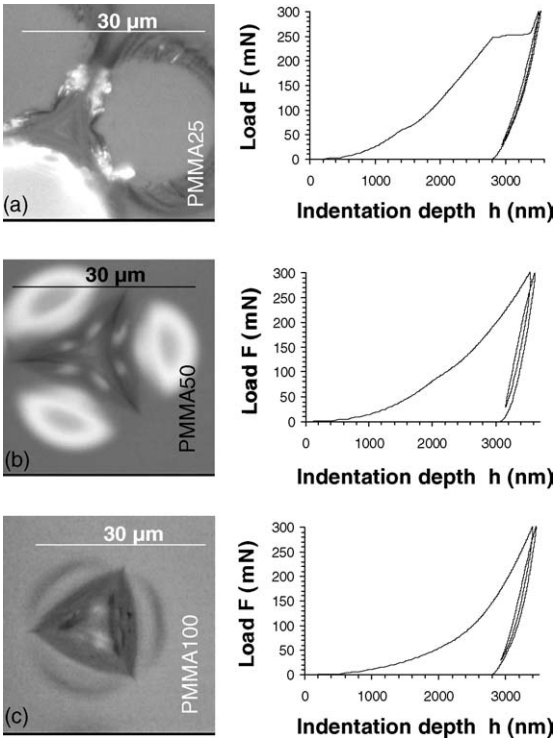

Fig. 8. Indentations into hybrid coatings observed using optical microscopy after applying loads of 300 mN and load–displacement curves for: (a) PMMA25, (b) PMMA50 and (c) PMMA100.

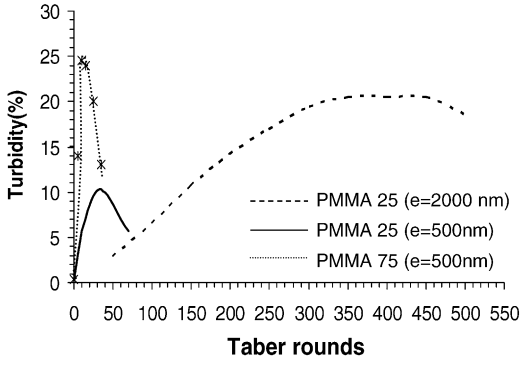

Fig. 9. Evolution of the turbidity of hybrid samples after Taber abrasion as a function of the number of revolutions.

4. Conclusion

Hybrid materials based on poly(methyl methacrylate) covalently linked to a silica network, produced from the in situ hydrolysis and condensation of an alcokysilane, have been elaborated. The mechanical properties of thin films, deposited by spin-coating, can be analyzed by nanoindentation tests. Different compositions of coatings have been studied and homogeneous interpenetrated networks have been obtained. All the hybrid coatings showed a time-dependent mechanical response, which can be considered by suitable procedures. Hence, reproducible indentation modulus and hardness values have been determined from the indentation curves and by using suitable models; they were in good agreement with the composition of the layers. All these results validate the nanoindentation measurements as an appropriate technique to study the mechanical properties of hybrid polymer-oxide thin films built from organic polymers cross-linked by inorganic nanodomains.

Acknowledgements

The authors want to thank Saint-Gobain Recherche for financial support and especially Laurent Delattre, Arnaud Huignard and Didier Lefèvre for helpful discussions, Laure Castel for SEM analyses and David Le Bellac for residual stress measurements.

References

1. Brinker, C. J. and Scherrer, G. W., *Sol–Gel Science—The Physics and Chemistry of Sol–Gel Processing*. San Diego, 1990.
2. Wilkes, G. L., Schaefer, D. W. and Mark, J. E., *Mat. Res. Soc. Symp. Proc.*, 1990, **171**, 15–29.
3. Abramoff, A. and Klein, L. C., *SPIE*, 1990, **1328**, 241–248.
4. Novak, B. M., *Adv. Mater.*, 1993, **5**(6), 422–433.
5. Sanchez, C. and Ribot, F., *New J. Chem.*, 1994, **18**(10), 1007–1047.
6. Huang, H.-H., Orler, B. and Wilkes, G. L., *Macromolecules*, 1987, **20**(6), 1322–1330.
7. Landry, C. J. T. and Coltrain, B. K., *Polymer*, 1992, **33**(7), 1486–1495.
8. Maï, C. and Perez, J., *First European Workshop on Hybrid Organic–Inorganic Materials (Synthesis, Properties Applications)*, 1993, 249–252.
9. Etienne, P., Phalippou, J. and Sempere, R., *J. Mater. Sci.*, 1998, **33**, 3999–4005.
10. Guermeur, C., Lambard, J., Gérard, J. F. and Sanchez, C., *J. Mater. Chem.*, 1999, **9**(3), 769–778.
11. Innocenzi, P., Esposto, M. and Maddalena, A., *J. Sol–Gel Sci. Technol.*, 2001, **20**, 293–301.
12. Malzbender, J., den Toonder, J. M. J., Balkenende, A. R. and de With, G., *Mater. Sci. Eng. R.*, 2002, **36**, 47–103.
13. Robertson, M. A., Rudkin, R. A., Parsonage, D. and Atkinson, A., *J. Sol–Gel Sci. Technol.*, 2003, **26**(1–3), 291–295.
14. Soloukhin, V. A., Posthumus, W., Brokken-Zijp, J. C. M., Loos, J. and de With, G., *Polymer*, 2002, **43**(23), 6169–6181.
15. Hajji, P., *Etude Des Relations Synthèse-Morphologie-Propriétés Mécaniques de Nanocomposites Hybrides Polymère-Silice: Application au Renforcement Mécanique des Verres*. Ph.D., Institute National des Sciences Appliquées, Lyon, 1999.
16. Frings, S., *Organic–Inorganic Hybrid Coatings Based on Polyester Resins and In Situ Formed Silica*. Ph.D., Technische Universiteit, Eindhoven, 1999.
17. Malzbender, J. and de With, G., *Thin Solid Films*, 2001, **386**(1), 68–78.
18. Delattre, L., *Caractérisation Structurale des Étapes D'élaboration Par Voie Sol–Gel de Matériaux Hybrides Organiques-Inorganiques*. Ph.D., Université Pierre et Marie Curie, Paris, 1996.
19. Stoney, G. G., *Proc. R. Soc. Lond.*, 1909, **A82**, 172–175.
20. Vella, J. B., Adhihetty, L. S., Junker, K. and Volinsky, A. A., *Int. J. Fract.*, 2003, **119/120**, 487–499.
21. Rouxel, T. and Sangleboeuf, J. C., *J. Non-Cryst. Solids*, 2000, **271**(3), 224–235.
22. Oliver, W. C. and Pharr, G. M., *J. Mater. Res.*, 1992, **7**(6), 1564–1583.
23. Aruchamy, A., Blackmore, K. A., Zelinski, B. J. J., Uhlmann, D. R. and Booth, C., *Mat. Res. Soc. Symp. Proc.*, 1992, **249**, 353–357.
24. Chang, T. C., Wang, Y. T., Hong, Y. S. and Chiu, Y. S., *J. Polym. Sci. (A) Polym. Chem.*, 2000, **38**, 1972–1980.
25. Lebeau, B., Maquet, J., Sanchez, C., Beaume, F. and Laupretre, F., *J. Mater. Chem.*, 1997, **7**(6), 989–995.
26. Mammeri, F., Rozes, L., LeBourhis, E. and Sanchez, C., *J. Sol–Gel Sci. Technol.*, 2003, **26**(1–3), 413–417.
27. Tang, B. and Ngan, A. H. W., *J. Mater. Res.*, 2003, **18**(5), 1141–1148.
28. Oyen, M. L. and Cook, R. F., *J. Mater. Res.*, 2003, **18**(1), 139–150.
29. Mammeri, F., Le Bourhis, E., Rozes, L. and Sanchez, C., *J. Non-Cryst. Solids*, 2004, **345–346**, 610–614.
30. Mencik, J., Munz, D., Quandt, E., Weppelmann, E. R. and Swain, M. V., *J. Mater. Res.*, 1997, **12**(9), 2475–2484.
31. Doerner, M. F. and Nix, W. D., *J. Mater. Res.*, 1986, **1**(4), 601–609.
32. Dériano, S., Rouxel, T., Malherbe, S., Rocherullé, J., Duisit, G. and Jézéquel, G., *J. Eur. Ceram. Soc.*, 2004, **24**, 2803–2812.
33. Bhattacharya, A. K. and Nix, W., *Int. J. Solids Struct.*, 1988, **24**, 1287–1298.